Effects of forest structure and airborne laser scanning point cloud density on 3D delineation of individual tree crowns

4 authors, including:

Kaja Kandare
FONDAZIONE EDMUND MACH - ISTITUTO AGR…
3 PUBLICATIONS **10** CITATIONS

Hans Ole Ørka
Norwegian University of Life Sciences (NMBU…
31 PUBLICATIONS **820** CITATIONS

Michele Dalponte
FONDAZIONE EDMUND MACH - ISTITUTO AGR…
36 PUBLICATIONS **832** CITATIONS

Some of the authors of this publication are also working on these related projects:

Project Forest biomass assessment in miombo woodlands using field and remote sensing techniques. View project

Project HyperBio View project

Effects of forest structure and airborne laser scanning point cloud density on 3D delineation of individual tree crowns

Kaja Kandare[1,2]*, Hans Ole Ørka[2], Jonathan Cheung-Wai Chan[1,3] and Michele Dalponte[4]

[1]FoxLab, Joint CNR-FEM Initiative, Fondazione E. Mach,
Via E. Mach 1, 38010, San Michele all'Adige (TN), Italy
[2]Department of Ecology and Natural Resource Management,
Norwegian University of Life Sciences, P.O. Box 5003, N-1432 Ås, Norway
[3]Department of Electronics and Informatics (ETRO), Vrije Universiteit Brussel,
Pleinlaan 2, 1050, Brussels, Belgium
[4]Department of Sustainable Agro-ecosystems and Bioresources, Research and Innovation Centre,
Fondazione E. Mach, Via E. Mach 1, 38010, San Michele all'Adige (TN), Italy
*Corresponding author, e-mail address: kaja.kandare@fmach.it

Abstract

This paper presents a 3D delineation method for airborne laser scanning point cloud. The method is based on an unsupervised clustering technique applied on horizontal slices followed by vertical merging based on overlapping among clusters. On an Alpine forest dataset, we analysed the effects of different forest structures and point cloud densities on tree crown delineation. Forest structure affects mainly the omission error, which eases with homogeneous tree spacing and sizes, while on the commission error forest structure has only slight effect. Delineation accuracy increases with higher point densities where Mann-Whitney-Wilcoxon test shows that accuracy differences between thinned data and original data are statistically significant.

Keywords: 3D delineation, ITC, ALS, point density, forest structure, alpine forest.

Introduction

Airborne laser scanning (ALS) data allows us to analyze large areas and to provide accurate up-to-date information about the composition, distribution and condition of forests. ALS data has become a common data source used for the estimation of forest biophysical attributes at stand level such as mean tree height, basal area (*BA*) and volume per hectare [Næsset, 2002], and also at tree level such as tree height, diameter at breast height (*DBH*) and stem volume [Hyyppä et al., 2001]. Individual trees are the basic and smallest unit on which forest management is carried out. The first processing step for tree-level inventories using ALS data is typically the delineation of individual tree crowns (ITCs). Then, for each ITC, attributes such as tree position, tree height, stem *DBH* and stem volume are estimated

[Hyyppä et al., 2001]. In inventory practice, many attributes have to be estimated at the tree level in order to be useful. Individual tree coordinates, for instance, are needed for harvesting operations and growth predictions [Pedersen et al., 2012]. ITC approaches are used also in operational urban tree mapping, and monitoring [Holopainen et al., 2013]. When combined with multispectral or hyperspectral images, ITC approaches could provide species information for each tree [Ørka et al., 2013]. Other recent works have shown that ITC delineation could provide supplementary information for area-based prediction of forest variables [Hyyppä et al., 2012] with reduce edge-effects [Packalen et al., 2015].

Numerous ITC detection methods for ALS data have been proposed in the last two decades [Hyyppä and Inkinen, 1999; Brandtberg et al., 2003; Solberg et al., 2006; Tang et al., 2007; Ferraz et al., 2012; Duncanson et al., 2014]. The first ITC delineation methods proposed in the literature used a 2D canopy height model (CHM) which is interpolated from the normalized ALS heights. Individual trees were delineated by defining a crown around local maximum. The most common 2D delineation methods are region growing [Hyyppä and Inkinen, 1999; Hyyppä et al., 2001; Solberg et al., 2006], multi-scale techniques [Persson et al., 2002; Brandtberg et al., 2003] or watershed segmentation [Tang et al., 2007; Ene et al., 2012]. However, the majority of these delineation methods can detect only trees that are well visible in the uppermost canopy layer, whereas intermediate and suppressed trees are rarely detected. Furthermore, while these 2D methods provided at times good results, the accuracy of delineated ITCs is strongly dependent on the quality of the CHM [Ene et al., 2012]. Indeed, generating a CHM from an ALS point cloud resulted in loss of information. Alternatively, if higher point density data are available, advanced 3D methods can refine the initial CHM-based delineation. 3D point clouds are often used to characterize a vertical structure of heterogeneous canopies. However, effective processing of high point density data is still a challenging task. Many methods delineated tree crowns by various 3D clustering analysis, namely: K-means [Morsdorf et al., 2004; Gupta et al., 2010], adaptive and agglomerative clustering [Lee et al., 2010; Gupta et al., 2010], mean shift clustering [Ferraz et al., 2012] and ellipsoidal clustering [Lindberg et al., 2014]. Some of these clustering methods were also combined with surface models or CHM. Other 3D delineation methods first generated a preliminary watershed segmentation of the CHM to define tree segments and afterwards separated trees within each segment by normalized cut segmentation [Shi and Malik, 2000] on the ALS point cloud [Reitberger et al., 2009], or by a trough-finding algorithm on the ALS height histogram [Duncanson et al., 2014]. Some delineation methods first delineated tree crowns on the 2D horizontal projection images at different height levels, and then the 'tree' segments delineated from various layers were combined to form 3D tree crowns [Wang et al., 2008; Tang et al., 2013]. Some 3D methods are very particular in their approach [Li et al., 2012; Lähivaara et al., 2014; Lu et al., 2014]. Li et al. [2012] delineated ITCs based on object-oriented classification rules such as tree proximity and shape criteria. Using a prior information on tree shapes Lähivaara et al. [2014] applied Bayesian estimation for 3D delineation. For identifying tree trunk points, Lu et al. [2014] used the ALS intensities and then points belonging to the same tree were defined by topology relationship.

While there are many 3D delineation methods proposed in the literature, they are not all adequately validated as important accuracy measures such as omission and commission errors, or errors are not reported [e.g. Gupta et al., 2010; Tang et al., 2013]. When an ITC

delineation method fail to detect individual trees present, it leads to omission errors. When one tree is split in multiple ITCs, it leads to a commission error. Many 3D methods seem to have a high commission error [Kaartinen et al., 2012; Eysn et al., 2015]. The absence of a well-established or benchmark method is making the comparison of performance among various methods difficult. Furthermore, few methods were tested in different forest conditions in terms of complexity. As forest structure usually affects the performance of delineation, its influence should be described and assessed using measures such as spatial arrangement, size variation of trees and structural diversity [Neumann and Starlinger, 2001; McElhinny et al., 2005; Lexerød and Eid, 2006; O'Hara et al., 2007].

New ALS technologies gather data at very high point density, which allows for development of 3D delineation methods. To our knowledge, no reported studies have analyzed the influence of point density higher than 30 pulses m^{-2} on ITC delineation. In this work, we tested a 3D delineation method for a very high-density ALS point cloud data (approx. 60 pulses m^{-2}). The forests are characterized by different structures: from mixed to pure stands, and from unevenly to evenly aged stands. Using field measurements, we evaluated the performances of the proposed 3D method in terms of delineation accuracy as well as tree attributes estimation. Finally, we qualitatively assessed the proposed method and compared it with a selected popular method (Reference delineation method). It would be important to evaluate the ITC delineation method with respect to various forest structures and point cloud densities. To this end, our objectives are two folds:

    i. to understand the effect of forest structure on the delineation performance;
    ii. to understand the effect of point density on the delineation performance.

Given the high point density made available to this study, we have the opportunity to assess the saturation of information intrinsic in ALS point cloud density with respect to tree delineation applications. Testing high-density ALS data may shed some light on whether it is worthwhile to acquire expensive high-density data for ITC studies.

Data set description
Study area
The 32 km^2 study area is located in the municipality of Pellizzano (46°17'22''N, 10°46'05''E) in the Italian Alps (Fig. 1). The forest structure is complex, with patches of mixed and pure tree species composition [Dalponte and Coomes, 2016]. Norway spruce (*Picea abies* (L.) H. Karst.) represents around 65% of the total stem volume, European larch (*Larix decidua* Mill.) around 25%, and the remaining 10% consists of other conifers (i.e. Silver fir (*Abies alba* Mill.), Swiss stone pine (*Pinus cembra* L.) and broadleaves (i.e. Silver birch (*Betula pendula* Roth), Common alder (*Alnus glutinosa* (L.) Gaertn.), Sycamore maple (*Acer pseudoplatanus* L.), Rowan (*Sorbus aucuparia* (L.) Crantz)). The topography varies considerably, with altitude ranging between 850 m and 2700 m and some areas characterized by very steep slopes. Vegetation varies from meadows in the higher parts of the study area to very dense forest in the lower parts. The area has been managed since 1950 with silvicultural plans carried out every 10 years. Selective logging is done with the help of cableway focusing on productive wood (e.g. Norway spruce). The harvesting methods are different depending on the forest structure and species present.
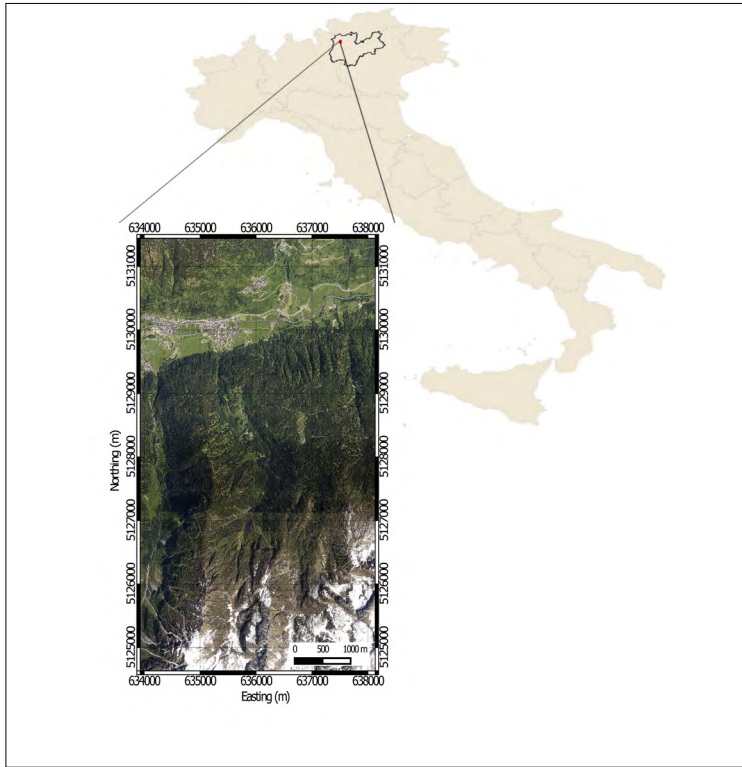
Figure 1 - Location of study area in Pellizzano, province of Trento in Italy.

Airborne Laser Scanner data

The data acquisition was carried out between 7th and 9th of September 2012 using a Riegl LMS-Q680i laser scanner. The system mounted on a Multi Mission Aircraft was optimized to measure canopy structure with a flying speed of about 51 m/s at an altitude of 660 m above ground level. The scan frequency was 400 kHz with a 60° field of view and the overlap for each stripe was at least 30%. Up to five returns were recorded for each emitted pulse and the mean point density was approximately 60 pulses m^{-2}. A Digital Terrain Model (DTM) was generated with TerraScan software with a grid size of 0.5 m. ALS point cloud was normalized to obtain a canopy height by subtracting the DTM from the z values of the ALS pulses. Figure 2a shows a common example of field plot and Figure 2b is an example of Norway spruces.

Field data

Field data were collected in the summers of 2013 and 2014. 14 plots were surveyed in forest stands with various structure and topography (mean slope is 20.4° with standard deviation at ± 6.7°). The plot radius was 15 m for six plots and 20 m for the remaining ones. The center location of each plot was measured with a GPS/GLONASS system resulting in a position error of less than 1 m. Furthermore, all trees on the plots were measured and the location was recorded as a reference to the center of the plot (azimuth and range). In total,

735 trees were measured across the plots. For each tree, the *DBH* along two orthogonal directions, the tree species, and the crown area were measured. Crown area was calculated from the field-measured distances north, south, east and west directions from the trunk center to the crown boundary assuming an ellipsoidal shape. Tree heights were measured on 66% of the trees using a Vertex III hypsometer. Tree heights for the remaining 34% trees were estimated with allometric equations [Scrinzi et al., 2010]. The allometric derived heights are overestimated compared to the field measured ones for 1.2 m with a RMSE of 2.35 m. The horizontal and vertical accuracies for an individual tree measurement are within ± 1 m error range. In each plot, only trees with a *DBH* greater than or equal to 5 cm were considered in the analyses. Dead or damaged trees without crown were excluded from further process. The total number of trees across all plots was 685. Table 1 summarizes the field data.
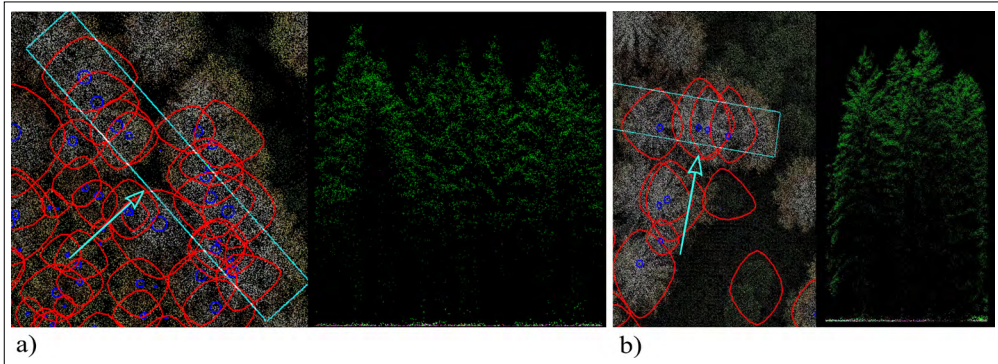

Figure 2 - a) Common plot structure. b) Group of four Norway spruces with five treetops. The last tree in the row has two tops growing from the same stem. On the left side of both figures there is a top view of the ALS point cloud. The light blue rectangles show the area of interest and the arrows show the view direction of the side view on the right side. The top view is overlaid with the field-measured stem positions marked with blue circles, and the field-measured tree crowns marked with red polygons. Polygons without stem position are bushes.

Table 1 - Summary of the field measurements at both tree and plot levels. *DBH* = Diameter at Breast Height (1.30 m), *BA* = basal area.

		Minimum	**Maximum**	**Mean**
Tree level	*DBH* [cm]	5.0	89.0	32.3
	Tree height [m]	2.5	39.8	21.5
	Crown area [m²]	0.03	123.70	17.06
	Number of stems/plot	11	132	49
Plot level	Mean *DBH* [cm]	21.7	58.1	36.7
	Number of stems/ha	127	1050	502
	Gini coefficient of *BA*	0.19	0.65	0.46
	BA [m²/ha]	35.7	77.8	55.0

Methods

3D delineation method

Figure 3 summarizes the four steps of the proposed 3D delineation method. In the preprocessing, the ALS point cloud with *X, Y, Z* coordinates is normalized and the ALS points with normalized *Z* coordinates (height) lower than 1.5 m are not used to avoid negative effects due to terrain objects and herbaceous vegetation. The point cloud is horizontally sliced. Within each slice, points are spatially clustered through several steps. The processes and parameters are described in detail in the following subsections.
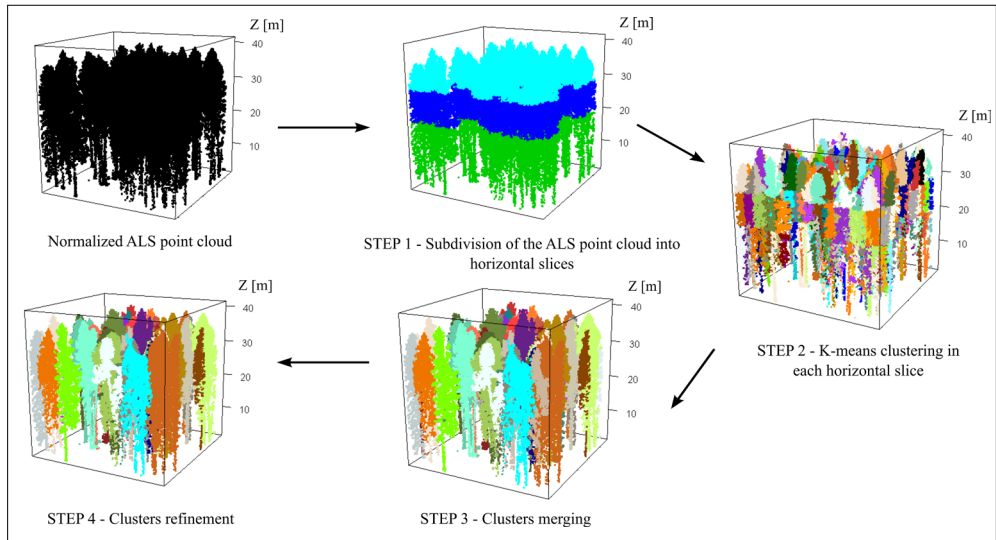

Figure 3 - Overview of the 3D individual tree crown delineation method. *Z* represents normalized heights of an ALS point cloud.

Step 1 - Subdivision of the ALS point cloud into horizontal slices

The initial point cloud is subdivided into three horizontal slices by Otsu thresholding [Otsu, 1979]. Otsu determines global thresholds which minimize the within-class variance. It is a popular method used by some ITC delineation studies for selecting threshold values [Ene et al., 2012; Dalponte et al., 2015].

Step 2 - K-means clustering in each horizontal slice

In each horizontal slice a CHM with 0.5 m resolution is created and a local maxima (LM) filtering is applied using a moving window with different sizes. The size of the moving window is user-defined and can vary for different horizontal slices. Using the position of the LM in each slice as centers, a K-means clustering algorithm is applied to generate clusters in each slice. We used the implementation of the R-package *stats* version 2.15.3. For each resulting clusters the *X* and *Y* cluster center coordinates are defined as arithmetic mean of *X* and *Y* coordinates of the points in each cluster.

As moving window is set empirically, a sensitivity analysis is carried out on three moving windows (ws) with the same sizes at each horizontal slice (Tab. 2). Based on the results of

the previous sensitivity analysis, we further inspected windows (w) (with different sizes among the three horizontal slices (Tab. 3).

Step 3 - Clusters merging

The K-means clusters are merged across all slices. The merging starts with the highest clusters (defined by the highest point of each cluster) as the tallest trees are well visible in the uppermost canopy layer. The lower clusters are assigned to the highest cluster if the 2D Euclidean distances between the lower cluster centers and the highest cluster center are within a predefined radius calculated as w*CHM. This radius value is defined differently depending on to which horizontal slice the highest cluster belongs to. Each iteration will start with a new highest cluster, which has not been already assigned to the previous highest clusters. At the end of all iterations, all initial K-means clusters with the same assignment are merged into the same cluster.

Table 2 - Combinations of four cubic moving window sizes.

	*ws*1	*ws*2	*ws*3	*ws*4
Top slice	11	9	7	5
Middle slice	11	9	7	5
Bottom slice	11	9	7	5

Table 3 - Combinations of four moving window sizes, altering the window size in different slices.

	*w*1	*w*2	*w*3	*w*4
Top slice	9	9	9	7
Middle slice	9	9	7	7
Bottom slice	9	7	7	7

Step 4 - Clusters refinement

Clusters resulted from Step 3 are sorted by height in the same way as in the previous step. Starting with the highest clusters, neighboring clusters are merged based on an overlapping area criterion. The overlapping area is defined as the percentage of the overlapping points with respect to the total number of points within the cluster. Overlapping percentage for both considered clusters are calculated and if any of the two overlapping percentages is higher than the threshold *OA*[%], they are merged. Otherwise, the next neighboring cluster with an overlapping is considered. The described procedure is repeated for all lower clusters and then the same process is replicated for the next highest cluster. All merging is completed at the end of this step. The resulting clusters are projected onto the horizontal plane. For each plot, an expected minimum crown area (*MinA*) is defined (e.g. 2 m²). If the projected crown area is smaller than *MinA*, the cluster is removed.

To better define the overlapping criterion for merging, we have carried out another sensitivity analysis to test *OA* thresholds from 40% up to 70%. The *MinA* used in this study is obtained from the field measurements (Tab. 1). The constraint was used to avoid clusters that are too small, which could be a result of noise. In the situation where the field reference data

are missing *MinA* can be approximated using a semivariogram analysis [Woodcock et al., 1988], a preliminary watershed segmentation, or by measurements recorded in a previous forest inventory.

Step 5 - Delineation of Individual Tree Crowns
The tree clusters represent ITCs, which are delineated as convex hulls. Tree attributes including tree position, tree height and crown area are generated. The ITC position *(X, Y)* and the tree height *(Z)* are extracted using the highest ALS point within a tree cluster. The crown area is computed as the convex hull of the *X* and *Y* coordinates of the tree cluster.

Reference delineation method
To generate a reference individual tree crown data set, we used a delineation method that exploits both CHM and ALS point cloud with normalized *Z* coordinates, implemented in the R-package *itcSegment*. First, a CHM is generated with a spatial resolution of 0.5 m using a nearest neighbor interpolation and then smoothed by a Gaussian low-pass filter (LPF) with a 3x3 moving window. A set of seed points $S=\{s_1,\ldots,s_N\}$ is defined using a filter based on local maxima. For pixels higher than 2.5 m, a LPF with a 5x5 moving window was used. A region map *L* is defined as $L_{i,j} = k$ if (*I, j*) is a seed point with index *k*, otherwise $L_{i,j} = 0$. Starting from *L*, regions grow according to the following procedure: considering a region map point $L_{i,j} \neq 0$ and taking its neighbor pixels in the CHM. A neighbor pixel is added to the region *n* if all three conditions are fulfilled: i) the distance between the neighbor pixel and the seed point s_n is smaller than 10 m; ii) the height of the considered neighbor pixel is greater than the height of the seed point s_n multiplied by a user-defined parameter called $Perc_{Tresh}$ varying between 0 and 1. The value was set to 0.7. This procedure is repeated until no more pixels are added to any regions. From each region the first returns are extracted and Otsu thresholding [Otsu, 1979] is applied to the normalized heights. Using first returns that are higher than the Otsu threshold, 2D convex hulls are generated from the *X* and *Y* coordinates to create the final ITCs.

Design of experiment
Accuracy assessment
For accuracy assessment, we followed the tree matching process introduced by Eysn et al. [2015]. If several field-measured trees matched with the same ITC derived from ALS data, only the one with shortest 2D distance and shortest height difference was compared. The performances of the delineation methods were evaluated using three delineation accuracy measures: omission error (*OE*), commission error (*CE*), and accuracy index (*AI*). The ratio between the number of field trees that were not delineated (C_F) and the actual number of field-measured trees (N_F) defined the *OE* [Eq.1]. The ratio between the number of ITCs that were not matched (C_{ITC}) with a field measurement and the number of field-measured trees (N_F) defined the *CE* [Eq. 2]:

$$OE = \frac{C_F}{N_F}100\% \quad [1]$$

$$CE = \frac{C_{ITC}}{N_F}100\% \quad [2]$$

The *AI* [Pouliot et al., 2005] incorporates both error types into a single metric:

$$AI = 100\% - \left(OE + CE \right) \quad [3]$$

The same accuracy measures were used in the sensitivity analysis. The setting of *w* and *OA*, which achieved the highest *AI* were selected for the remaining experiments.

The accuracy of tree attributes was assessed for the *n* correctly detected trees by mean differences (*MD*) and Root-mean-square errors (*RMSE*) as:

$$MD = \frac{\sum_{i=1}^{n} e_i}{n} \quad [4]$$

$$RMSE = \sqrt{\frac{\sum_{i=1}^{n} e_i^2}{n}} \quad [5]$$

where e_i for the tree height and crown area was calculated as the difference between the field-derived and the ALS-derived estimates. For the tree position, e_i was computed by Euclidean distance between the field measurement and the ALS estimated position. The relationship between ITC attributes estimated from the ALS data and the field measurements was assessed by coefficient of determination (r^2) (or square of the Pearson correlation coefficient). We also qualitatively evaluated our results against the Reference delineation method that was proved to work successfully in a comparative study in Alpine forests as Method 2 described in Eysn et al. [2015].

Forest structure

Forest structure refers to attributes that quantify the forest such as spatial arrangement and size of trees. We selected four measures to characterize forest structure: mean *DBH*, number of stems per hectare, mean nearest neighbor distance and Gini coefficient of basal area. *DBH* is a measure of tree size and the number of stems per hectare is a measure of density. Furthermore, mean nearest neighbor distance is used to describe the variation of tree spacing. Structural diversity which is related to dimeter distribution can be assessed with different indices (e.g. Shannon index, Simpson index, Gini coefficient). On the basis of previous studies the Gini coefficient was found to be the most suitable [Lexerød and Eid, 2006; O'Hara et al., 2007]. We used the Gini coefficient [Gini, 1912] to describe the level of homogeneity or heterogeneity of the forest [Bollandsås et al., 2008]. The Gini coefficient values are bound between zero (indicating homogeneous) and one (indicating heterogeneous). Hence, uneven aged stands would have higher Gini coefficient values than even aged stands.

Data thinning

In order to test the robustness of the 3D delineation method with low point densities, the original ALS data (with mean pulse density of 60 pulses m^{-2}) were thinned. In particular, the following mean point densities were considered: 50, 30, 20, 10, 6 and 4 pulses m^{-2} (Fig. 4). The data thinning of ALS data was executed on pulse level using the module *lasthin* of the LAStools software, a popular tool to test effects of point density on forest attributes [Jakubowski et al., 2013]. To maintain the fairly regular spatial distribution of the ALS pulses, the thinning was performed on randomly selected points from different grid sizes to obtain lower point densities. A similar approach was used by Hansen et al. [2015]. The thinning of each point density was repeated ten times and our delineation method was applied to each of the ten thinnings. At the end, the average delineation accuracy of ten thinnings in terms of *AI* was calculated. To test if the differences among accuracies obtained with thinned and original data were significant, we carried out a two-sided Mann-Whitney-Wilcoxon test.
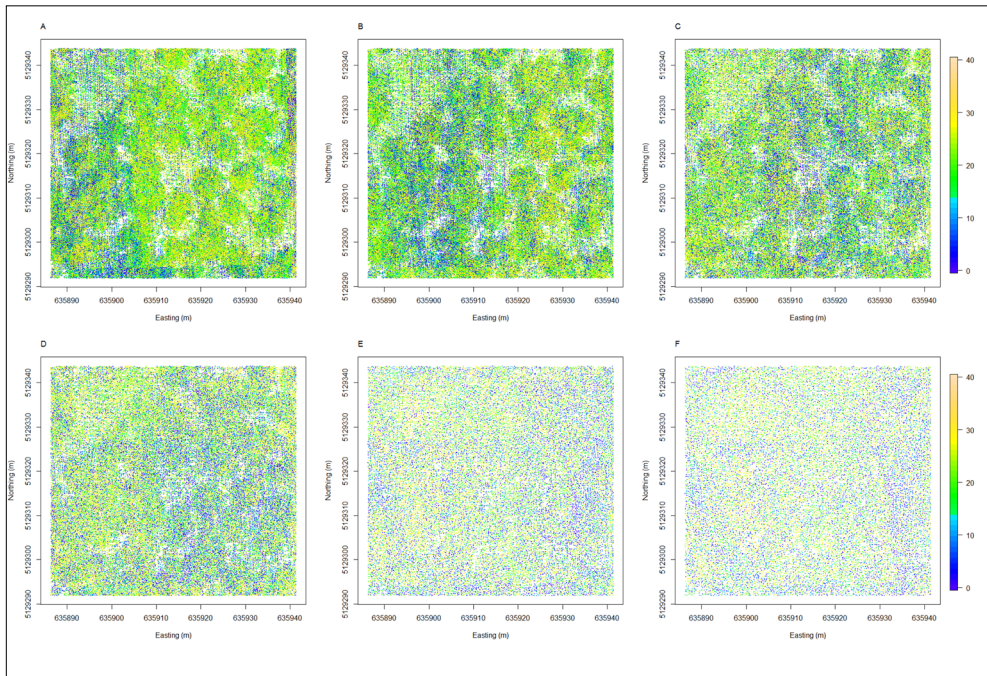

Figure 4 - The area of a plot with different pulse densities: a) 60 pulses m^{-2}; b) 30 pulses m^{-2}; c) 20 pulses m^{-2}; d) 10 pulses m^{-2}; e) 6 pulses m^{-2}; f) 4 pulses m^{-2}.

Results

Sensitivity analysis

To understand the relationship between accuracy and window size for initial clustering, we started with cubic windows or a box where window size was the same in all three slices (Tab. 2). According to Popescu et al. [2002] if the window size is too large, the

delineation method tends to have higher *OE*. On the opposite if the window size is too small, the delineation method tends to have higher *CE*. Our results in Table 4 confirmed the findings of abovementioned report and showed that the best compromise between *OE* and *CE* was obtained by moving windows *ws*2 (9, 9, 9) and *ws*3 (7, 7, 7), which reached substantially higher *AI* (around 34%) than *ws*1 (11, 11, 11) and *ws*4 (5, 5, 5). Assuming that the uppermost canopy layer has a high pulse density and larger crowns, the clusters of pulses on the top slice should be larger. The pulse density drops below the canopy and so the crown size, thus the clusters of pulses should be smaller in the lower slices. Thus, we decided to investigate several configurations of *w* where window size format for lower slices are smaller resembling a vertical pulse density distribution scenario that could be more appropriate and corresponding to the geometry of a tree. Table 3 lists the experimented configurations *w* (*bottom, middle, top*): *w*1 (9, 9, 9), *w*2 (7 ,9, 9), *w*3 (7, 7, 9) and *w*4 (7, 7, 7). Table 5 presents the sensitivity analysis results for the original point density at 60 pulses per m^{-2} for window sizes from *w*1 to *w*4 and for overlapping area from 40% to 70%. From Table 5 it is evident that an increase of the overlapping area from 40% to 70% increases the *CE* and decreases the *OE*. In terms of overlapping, both 50% and 60% provided the best results. If we would exclude *w*4 where the range of accuracy for different overlappings are significantly higher, the *AI* differences for other window sizes for different overlappings are only marginal at around 1% or less. The *CE* and *OE* of different window configurations showed expected tendency as above-mentioned. However, altering window size at lower slices did not lead to higher delineation accuracy and there were no other patterns observed. As the combination of window size *w*1(9, 9, 9) and overlapping area at 50% had the highest accuracy, it was chosen as the setting for the remaining analysis.

The sensitivity analysis for the thinned data was also performed. The highest accuracies are highlighted in Tables 6 to 11. For each of the thinned point densities we produced ten random thinnings. For each parameter combination, the mean *AI* is showed. It emerged that window sizes *w*1, *w*2, and *w*3 reached quite similar results with overlapping areas at 40% and 50%, and their differences were within the range of around 1%.

Table 4 - Omission error (*OE* [%]), commission error (*CE* [%]), accuracy index (*AI* [%]) and number of detected ITCs (N) on the original point cloud carried out with different window sizes (*w*(*slice$_{low}$, slice$_{middle}$, slice$_{top}$*)) and overlapping areas (*OA*).

	*ws*1 (11, 11, 11)				*ws*2 (9, 9, 9)				*ws*3 (7, 7, 7)				*ws*4 (5, 5, 5)			
OA	*OE*	*CE*	*AI*	*N*	*OE*	*CE*	*AI*	*N*	*OE*	*CE*	*AI*	*N*	*OE*	*CE*	*AI*	*N*
40%	74.3	1.8	23.9	156	64.0	3.2	32.9	222	53.5	14.5	32.3	353	37.6	59.5	2.9	720
50%	70.5	2.4	27.2	179	60.3	5.5	34.3	256	51.4	18.3	30.4	392	34.6	71.8	-6.3	812
60%	69.2	2.8	27.9	189	58.5	7.5	34.0	275	50.1	23.8	26.1	428	33.2	78.5	-11.7	862
70%	68.9	3.7	27.4	195	57.8	9.3	32.9	290	48.5	27.3	24.2	458	32.3	85.5	-17.8	907

Table 5 - Omission error (*OE* [%]), commission error (*CE* [%]) and accuracy index (*AI* [%]) on the original point cloud carried out with different window sizes (*w*(*slice*$_{low}$, *slice*$_{middle}$, *slice*$_{top}$)) and overlapping areas (*OA*).

	w1 (9, 9, 9)			*w2* (7, 9, 9)			*w3* (7, 7, 9)			*w4* (7, 7, 7)		
OA	*OE*	*CE*	*AI*	*OE*	*CE*	*AI*	*OE*	*CE*	*AI*	*OE*	*CE*	*AI*
40%	64.0	3.2	32.9	63.2	3.7	33.1	61.9	5.6	32.4	53.5	14.5	32.3
50%	60.3	5.5	34.3	60.7	5.8	33.5	58.4	8.3	33.3	51.4	18.3	30.4
60%	58.5	7.5	34.0	59.6	7.1	33.3	56.4	9.8	33.8	50.1	23.8	26.1
70%	57.8	9.3	32.9	58.7	8.8	32.6	55.3	12.2	32.6	48.5	27.3	24.2

Table 6 - Accuracy index (*AI* [%]) obtained by sensitivity analysis for point density of 4 pulses m^{-2} carried out with different parameter settings (*w*(*slice*$_{low}$, *slice*$_{middle}$, *slice*$_{top}$) = window size, *OA* = overlapping area).

OA	*w1* (9, 9, 9)	*w2* (7, 9, 9)	*w3* (7, 7, 9)	*w4* (7, 7, 7)
40%	**28.2**	28.0	27.6	24.8
50%	27.5	27.5	27.7	23.1
60%	27.4	27.0	27.0	22.1
70%	27.0	26.7	26.6	21.4

ITC delineation

The results of *OE*, *CE* and *AI* of the proposed and the Reference delineation method were presented as the average over all plots. The delineation accuracy in terms of *OE*, *CE* and *AI* for the proposed method were 60.3%, 5.5%, 34.3%, respectively; for the Reference delineation method, they were 57.4%, 8.6%, 34.0%, respectively. In summary, there was only a marginal difference in terms of *AI* between the proposed 3D method and the Reference delineation method, with the 3D method achieving lower *CE* with slightly higher *OE*.

Table 7 - Accuracy index obtained by sensitivity analysis for point density of 6 pulses m^{-2} carried out with different parameter settings (*w*(*slice*$_{low}$, *slice*$_{middle}$, *slice*$_{top}$) = window size, *OA* = overlapping area).

OA	*w1* (9, 9, 9)	*w2* (7, 9, 9)	*w3* (7, 7, 9)	*w4* (7, 7, 7)
40%	28.8	28.9	28.8	25.7
50%	**29.0**	28.5	28.8	23.2
60%	28.7	28.2	27.9	21.9
70%	27.8	27.8	27.4	21.4

Table 8 - Accuracy index obtained by sensitivity analysis for point density of 10 pulses m^{-2} carried out with different parameter settings (w($slice_{low}$, $slice_{middle}$, $slice_{top}$) = window size, OA = overlapping area).

OA	w1 (9, 9, 9)	w2 (7, 9, 9)	w3 (7, 7, 9)	w4 (7, 7, 7)
40%	28.9	28.8	**30.0**	26.4
50%	29.2	28. 9	29.2	23.8
60%	28.6	27.9	28.4	21.9
70%	28.2	27.5	27.6	20.0

Table 9 - Accuracy index obtained by sensitivity analysis for point density of 20 pulses m^{-2} carried out with different parameter settings (w($slice_{low}$, $slice_{middle}$, $slice_{top}$) = window size, OA = overlapping area).

OA	w1 (9, 9, 9)	w2 (7, 9, 9)	w3 (7, 7, 9)	w4 (7, 7, 7)
40%	29.3	**30.2**	29.7	25.9
50%	29.4	29.7	29.6	23.3
60%	28.7	28.2	28.4	21.5
70%	27.1	26.8	27.3	19.7

Table 10 - Accuracy index obtained by sensitivity analysis for point density of 30 pulses m^{-2} carried out with different parameter settings (w($slice_{low}$, $slice_{middle}$, $slice_{top}$) = window size, OA = overlapping area).

OA	w1 (9, 9, 9)	w2 (7, 9, 9)	w3 (7, 7, 9)	w4 (7, 7, 7)
40%	30.1	29.9	29.5	27.5
50%	**30.6**	30.1	29.6	25.2
60%	29.9	29.1	29.2	23.0
70%	28.8	28.3	28.2	21.0

Table 11 - Accuracy index obtained by sensitivity analysis for point density of 50 pulses m^{-2} carried out with different parameter settings (w($slice_{low}$, $slice_{middle}$, $slice_{top}$) = window size, OA = overlapping area).

OA	w1 (9, 9, 9)	w2 (7, 9, 9)	w3 (7, 7, 9)	w4 (7, 7, 7)
40%	29. 9	30.8	30.7	29.4
50%	30.2	30.8	**31.0**	27.8
60%	29.5	30.0	30.3	25.4
70%	29.0	29.3	29.4	22.5

ITC attributes estimation

For the correctly delineated ITCs the accuracies of tree position, crown area and tree height are showed in Table 12. The accuracies of the tree positions estimated by the proposed 3D delineation method and the Reference delineation method were 2.13 m and 2.33 m, respectively. Regarding the crown area the 3D method overestimated its value ($MD = 9.77$ m^2) while the Reference delineation method achieved better results ($MD = 5.86$ m^2) with a small underestimation. The correlation between the two ALS-derived crown areas and field measurements were low, with r^2 at 0.17 for the 3D methods and 0.20 for the Reference method. For the estimation of tree heights, both methods reached the same r^2 at 0.96. The proposed 3D method overestimated the tree heights by 0.79 m and the Reference delineation method underestimated them by 0.48 m.

Table 12 - Accuracy of tree position, crown area and tree height for the 3D and Reference delineation method. Only ITCs matching a field measured tree are considered. MD = Mean Difference, $RMSE$ = Root Mean Square Error, r^2 = coefficient of determination.* Mean distance of the field tree position and the ITC position.

Method	3D delineation method			Reference delineation method		
	MD	*RMSE*	*r²*	*MD*	*RMSE*	*r²*
Tree position* [m]	1.54	2.13	-	1.89	2.33	-
Crown area [m²]	-9.77	47.77	0.17	5.86	15.69	0.20
Tree height [m]	-0.79	1.54	0.96	0.48	1.43	0.96

Effect of forest structure

The forest structure was described by four measures: Gini coefficient of *BA*, mean *DBH*, number of stems per hectare, and mean nearest neighbour distance. Figure 5 displays their effects on the delineation accuracy in terms of *OE* and *CE*. For the Gini coefficient of *BA* and mean *DBH*, it is evident that two major groups of plots are formed. The first group represented by the symbols ● and ■ has the heterogeneous Gini coefficient of *BA* above 0.5 and greater mean *DBH* above 42 cm. It represents mixed tree species within a plot containing uneven aged coniferous (Norway spruce, Larch and Silver fir) and broadleaves (Common alder, Sycamore maple, Silver Birch, European Birch, Rowan and Aspen). A second group represented by ○ and □ belongs to homogeneous tree species plots with even aged coniferous trees. The *OE* was higher for the mixed trees species plots than for the homogeneous tree species plots, wherein the *CE* was similar for both. From the number of stems per hectare and their mean nearest neighbour distance, we can see how the horizontal distribution of trees and the tree spacing affect the delineation accuracy. For the heterogeneous group of plots, a high number of stems per hectare and a low mean nearest neighbor distance resulted in higher *OE*. The second group of plots with less trees per hectare and a larger tree spacing resulted in lower *OE*. Unlike the *OE*, *CE* is very similar for most plots in both groups. Lastly, for each forest structure measure we fitted a linear regression model to *OE*s and *CE*s (Fig. 5). All forest structure measures have a significant relationship at significance level of 0.05 with *OE* but their relationship is not significant with *CE*. Thus, the forest structure measures affected the accuracy of ITC delineation and had more influence on *OE* than *CE*.
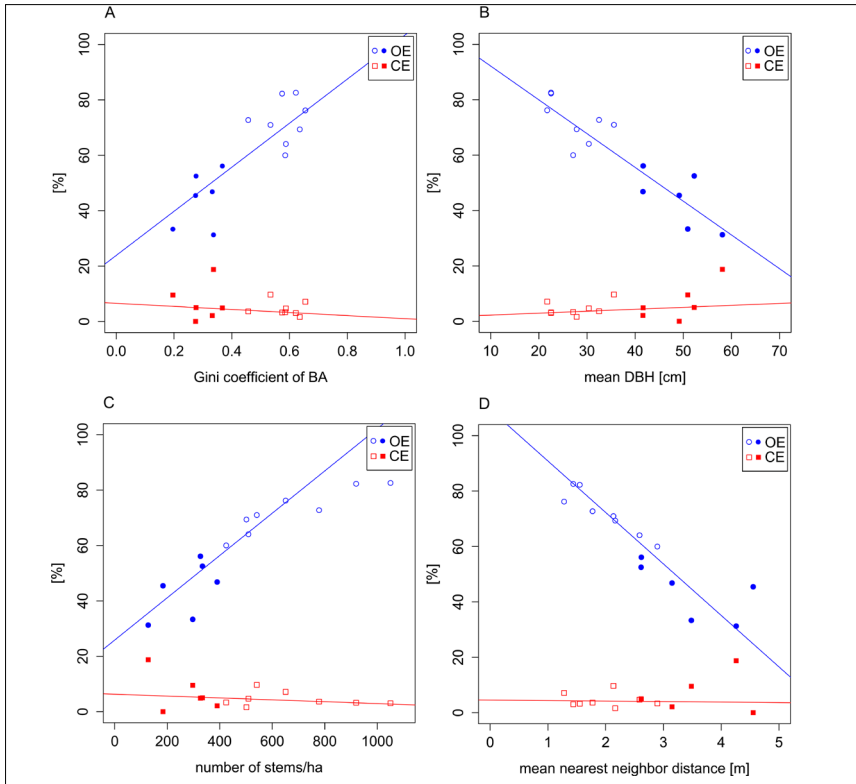
Figure 5 - Effect of forest structure in terms of (A) Gini coefficient of basal area (*BA*), (B) mean *DBH*, (C) number of stems per hectare and (D) mean nearest neighbor distance, on the omission errors (*OE*) and commission errors (*CE*). The blue circles and red squares represent the results of *OE* and *CE*, respectively. Each symbol represents the value of each plot and the solid lines are fitted with ordinary linear regression. The filled signs represent homogeneous plots in contrast to the empty signs representing heterogeneous plots.

Effect of point density

Figure 6 shows the performance of the proposed 3D delineation method in terms of *AI*, *OE* and *CE* at seven different point densities. For each point density, the best performing parameters were chosen based on sensitivity analysis. The mean values and standard deviation bars for each of the thinnings were calculated over ten random repetitions. Overall, from a point density of 4 pulses m^{-2} until a point density of 60 pulses m^{-2} the *AI* increased by 6.1% (Fig. 6). The results suggest that with a higher point density a higher delineation accuracy is reached. To test if the differences of delineation accuracies (*AI*) between different point density data sets were statistically significant, we performed a Mann-Whitney-Wilcoxon test at α = 0.05 level (Fig. 7). The outcome showed the differences between the accuracies of the original point density (60 points m^{-2}) and the thinned data sets are all significant. The difference in accuracy is also significant in most cases between 4 points m^{-2} and the other thinned data sets (except for 6 points m^{-2}). Moreover, it is also significant between thinned data set at 6 points m^{-2} and data sets at 30 and 50 points m^{-2}.
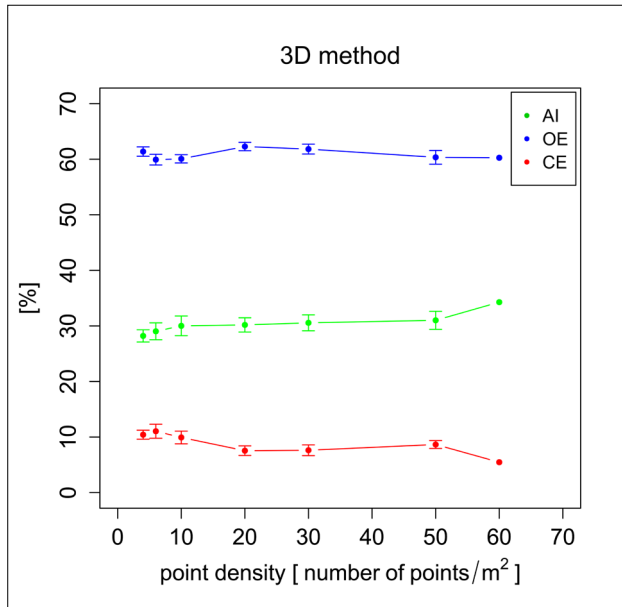
Figure 6 - Performance of the 3D delineation method at different point densities. The blue, red and green circles represent the results of the omission error (*OE*), commission error (*CE*) and accuracy index (*AI*), respectively. For each point density ten repetitions of thinning were carried out and their mean values and the standard deviation bars are presented.
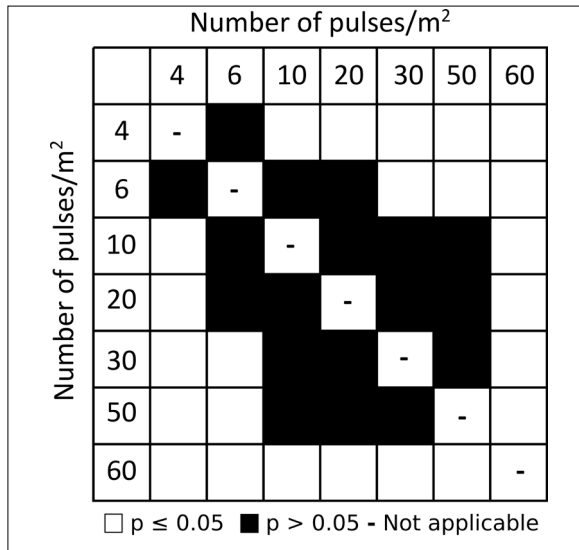

Figure 7 - Mann-Whitney-Wilcoxon test for the pairwise accuracy indexes at different point densities with □ represents significant and ■ represents not significant.

Discussion

The presented 3D delineation method has two important parameters: the size of moving window and the overlapping area (*OA*). The moving window can be adapted in each horizontal slice and the a priori knowledge of the expected crown size of a plot can be used as constraint. Local knowledge of the crown size can be obtained from field measurements or by prediction based on tree height if an allometric equation exists [Popescu et al., 2002]. The sensitivity analysis for the window sizes was done on two stages. Firstly, we tested cubic windows (*ws*) where window size was kept constant for each slice and then we refined the analysis only using the sizes that were providing the best results. The output of the first stage was that windows *ws*1 (11, 11, 11) and *ws*4 (5, 5, 5) were not suitable, as they provided quite low accuracies. Thus, in the second stage we considered only 9 and 7 as possible window dimensions and we defined a new configuration (*w*) with smaller window sizes for the slices at the lower heights: *w*1 (9, 9, 9), *w*2 (7, 9, 9), *w*3 (7, 7, 9), *w*4 (7, 7, 7). The new configuration of window size was based on the assumption that less points are gathered at lower level and that crowns are usually smaller under the canopy cover. From the results of the sensitivity analysis on the original point density, we concluded that the window size (*w*) had greater impact on the 3D delineation accuracy than the overlapping area (*OA*). Moreover, the range of *AI*s obtained at different window sizes is quite large, while the variations of *AI*s obtained at different overlapping areas (%) are actually quite small. In general, the best results were obtained by *w*1 (9, 9, 9) and *OA* 50%, though the accuracy of *w*1, *w*2, *w*3, at *OA* 50% and 60% were very similar. For thinned data the sensitivity analysis revealed that the window sizes *w*1, *w*2 and *w*3, with overlapping at 40% and 50% reached similar and the highest accuracies. It is worth noting that, the best window sizes for point densities 10, 20 and 50 pulses per m^{-2} were not *w*1 (9, 9, 9), even if the differences in accuracy were very marginal (from Tab. 6 to Tab. 11).

For the original point density data the proposed 3D delineation method and the Reference delineation method provided very similar results. The accuracies of both delineation methods are in line to those reported in other studies in coniferous and broadleaved forests [Vauhkonen et al., 2011], Alpine spruce and mixed forests [Reitberger et al., 2009], and different Alpine forests [Eysn et al., 2015].

Regarding the ITC attributes estimation, the 3D delineation and the Reference delineation methods achieved similar accuracies. Even with high point density data, the obtained tree position accuracy was not high. The relatively high tree position error can be explained either by the complex structure of our study area which is challenging (e.g. tilted trees, crown shape, high stem density) (Fig. 2), or by errors occurred in the field measurements of the plot position with GNSS, or by the complex topography (e.g. steep slope) [Monnet and Mermin, 2014]. Particularly on a steep slope higher than 20°, where the treetops are likely to be tilted to the valley side, a horizontal positional difference between the treetop and its stem could be possible. Steep slopes can also lead to an overestimation of ALS derived tree height, because the tree height is calculated as the distance between the tree top (highest normalized point inside the cluster) and the ground surface below the tree top point [Hollaus et al., 2006; Kaartinen et al., 2012]. Thus, the ALS data and the error inherited in the generation of DTM from the ALS point clouds are less precise in steep terrain [Hollaus et al., 2006]. Another error in height estimation can be related to the field-derived measurements, either caused by the error of allometric equation used, or

by subjectivity in the field measurements with Vertex hypsometer [Kitahara et al., 2010; Vasilescu, 2013]. Kitahara et al. [2010] found that the mean percentage difference of tree height measurements repeated three times by different surveyors are 3.6% for coniferous trees and 8.7% for broadleaves.

Tree heights obtained by the 3D delineation method were overestimated by 0.79 m and those obtained by the Reference delineation method were underestimated by 0.48 m. Such difference is caused by different ways of extraction of tree crown pulses. The 3D method extracted tree height as the highest pulse within an ITC cluster. The Reference method extracted tree height at 95th percentile of all heights within an ITC segment. The crown area was overestimated by the 3D delineation method and underestimated by the Reference method. The Reference delineation method defined a height threshold above which all first return pulses were accounted for crown area computation. While the proposed method simply took all pulses in a cluster for crown area calculation. In summary, the accuracy of tree attributes estimated by both methods are at good level as compared to previous studies [e.g. Kaartinen et al., 2012; Eysn et al., 2015].

Analyzing the effect of four forest structure measures on delineation accuracy, we find that pure tree species and even aged plots achieved lower *OE* as compared to mixed tree species and uneven aged plots. Comparing with pure tree species and even aged plots, the plots with mixed tree species and uneven ages in general had a higher Gini coefficient of *BA*, a higher number of stems per hectare, a smaller mean *DBH* and a smaller mean nearest neighbour distance between trees, which clearly led to higher *OE*. The *CE*, however, did not vary so much among different forest structures. In a related study, Eysn et al. [2014] reported that delineation accuracies with the Pellizzano test site were also comparatively low possibly caused by the high forest structure diversity.

The point density analysis revealed that the delineation accuracy of the 3D delineation method is higher with the original density at 60 pulses m^{-2} (Fig. 6). Previous studies concluded that point densities higher than 20 pulses m^{-2} did not have an important effect on the delineation results [Reitberger et al., 2009; Kaartinen et al., 2012; Yao et al., 2014]. Kaartinen et al. [2012] reported that increasing point density from 2 and 4 pulses m^{-2} to 8 pulses m^{-2} had only marginal improvement on delineation accuracy. The studies of Reitberger et al. [2009] and Yao et al. [2014] concluded that a point density higher than 10 pulses m^{-2} did not improve the performances of ITC delineation. However, Kaartinen et al.'s [2012] study focused mainly on 2D methods based on CHM, where the vertical structure was not explored. In our tests, the delineation accuracy increased with higher point density and it achieved marginal improvements when we increased the point density from 10 to 50 pulses m^{-2}. The Mann-Whitney-Wilcoxon test showed that differences in accuracy among the thinned datasets are not statistically significant at α = 0.05 between point densities 6, 10, 20, 30 and 50 pulses m^{-2}, except between point densities 6 m^{-2} and 30 pulses m^{-2}, and 6 m^{-2} and 50 pulses m^{-2}. This indicates the increase of point density from 6 to 50 pulses m^{-2} does not lead to interesting improvement in accuracy. The highest accuracy is achieved with the original point density (60 points m^{-2}) and the improvement in accuracy is tested significantly different when compared to all other thinned data sets. Simulation of thinned data by reducing a high-density ALS datasets are frequently used to give insight into the effect of point density [Magnussen et al., 2010; Jakubowski et al., 2013; Hansen et al., 2015]. However, we have to acknowledge thinning is only a simulation of the expected real

ALS flight at lower densities. An ideal option would be to obtain different point densities with the same scanner.

Conclusions

In this paper, a 3D ITC delineation method based on ALS data was presented and evaluated. The results were compared with a well-established Reference delineation method. Both methods reached similar delineation accuracies and both were effective in tree attributes estimation. We found that forest structure attributes such as stem density, distribution of trees, number of stems per hectare, and the evenness expressed by Gini coefficient of basal area, had significant influence on the delineation accuracy. We also observed that the omission error was lower in stands with a homogeneous forest structure and that the forest structure only had a slight effect on the commission error. In addition, due to the complex forest structure of our study site, the results have demonstrated that the proposed 3D delineation method was flexible and suitable to be applied in different forest conditions. Our method was robust and effective even with low point densities. Our thinning experiments have shown that the delineation accuracy was similar for point densities varying from 10 to 50 points m^{-2}. Overall, the delineation accuracy improved when the point density was increased and the top accuracy was achieved with the highest density at 60 points m^{-2}.

Acknowledgements

References

Bollandsås O.M., Buongiorno J., Gobakken T. (2008) - *Predicting the growth of stands of trees of mixed species and size: A matrix model for Norway.* Scandinavian Journal of Forest Research, 23: 167-178. doi: http://dx.doi.org/10.1080/02827580801995315.

Brandtberg T., Warner T.A., Landenberger R.E., McGraw J.B. (2003) - *Detection and analysis of individual leaf-off tree crowns in small footprint, high sampling density lidar data from the eastern deciduous forest in North America*. Remote Sensing of Environment, 85: 290-303. doi: http://dx.doi.org/10.1016/S0034-4257(03)00008-7.

Dalponte M., Coomes D.A. (2016) - *Tree-centric mapping of forest carbon density from airborne laser scanning and hyperspectral data*. Methods in Ecology and Evolution. doi: http://dx.doi.org/10.1111/2041-210X.12575.

Dalponte M., Reyes F., Kandare K., Gianelle D. (2015) - *Delineation of individual tree crowns from ALS and hyperspectral data: a comparison among four methods*. European Journal of Remote Sensing, 48: 365-382. doi: http://dx.doi.org/10.5721/EuJRS20154821.

Duncanson L.I., Cook B.D., Hurtt G.C., Dubayah R.O. (2014) - *An efficient, multi-layered crown delineation algorithm for mapping individual tree structure across*

multiple ecosystems. Remote Sensing of Environment, 154: 378-386. doi: http://dx.doi.org/10.1016/j.rse.2013.07.044.

Ene L., Næsset E., Gobakken T. (2012) - *Single tree detection in heterogeneous boreal forests using airborne laser scanning and area-based stem number estimates*. International Journal of Remote Sensing, 33: 5171-5193. doi: http://dx.doi.org/10.1080/01431161.2012.657363.

Eysn L., Hollaus M., Lindberg E., Berger F., Monnet J.-M., Dalponte M., Kobal M., Pellegrini M., Lingua E., Mongus D., Pfeifer N. (2015) - *A benchmark of lidar based single tree detection methods using heterogeneous forest data from the Alpine space*. Forests, 6: 1721-1747. doi: http://dx.doi.org/10.3390/f6051721.

Eysn L., Hollaus M., Monnet J.M., Dalponte M., Kobal M., Pellegrini M., Lindberg E., Mongus D., Berger F. (2014) - *NEWFOR Single Tree Detection Benchmark - report*. Wien, Austria.

Ferraz A., Bretar F., Jacquemoud S., Gonçalves G., Pereira L., Tomé M., Soares P. (2012) - *3-D mapping of a multi-layered Mediterranean forest using ALS data*. Remote Sensing of Environment, 121: 210-223. doi: http://dx.doi.org/10.1016/j.rse.2012.01.020.

Gini C. (1912) - *Variabilità e mutabilità contributo llo studio delle distribuzioni e delle relazioni statistiche*. Cuppini P. (Ed.), Bologna, 156 pp.

Gupta S., Weinacker H., Koch B. (2010) - *Comparative analysis of clustering-based approaches for 3-D single tree detection using airborne fullwave lidar data*. Remote Sensing, 2: 968-989. doi: http://dx.doi.org/10.3390/rs2040968.

Hansen E.H., Gobakken T., Næsset E. (2015) - *Effects of pulse density on digital terrain models and canopy metrics using airborne laser scanning in a tropical rainforest*. Remote Sensing, 7: 8453-8468. doi: http://dx.doi.org/10.3390/rs70708453.

Hollaus M., Wagner W., Eberhöfer C., Karel W. (2006) - *Accuracy of large-scale canopy heights derived from LiDAR data under operational constraints in a complex alpine environment. ISPRS* Journal of Photogrammetry and Remote Sensing, 60: 323-338. doi: http://dx.doi.org/10.1016/j.isprsjprs.2006.05.002.

Holopainen M., Kankare V., Vastaranta M., Liang X., Lin Y., Vaaja M., Yu X., Hyyppä J., Hyyppä H., Kaartinen H., Kukko A., Tanhuanpää T., Alho P. (2013) - *Tree mapping using airborne, terrestrial and mobile laser scanning - A case study in a heterogeneous urban forest*. Urban Forestry and Urban Greening, 12: 546-553. doi: http://dx.doi.org/10.1016/j.ufug.2013.06.002.

Hyyppä J., Inkinen M. (1999) - *Detecting and estimating attributes for single trees using laser scanner*. The Photogrammetric Journal of Finland, 16: 27-42.

Hyyppä J., Kelle O., Lehikoinen M., Inkinen M. (2001) - *A segmentation-based method to retrieve stem volume estimates from 3-D tree height models produced by laser scanners*. IEEE Transactions on Geoscience and Remote Sensing, 39: 969-975. doi: http://dx.doi.org/10.1109/36.921414.

Hyyppä J., Yu X., Hyyppä H., Vastaranta M., Holopainen M., Kukko A., Kaartinen H., Jaakkola A., Vaaja M., Koskinen J., Alho P. (2012) - *Advances in forest inventory using airborne laser scanning*. Remote Sensing, 4: 1190-1207. doi: http://dx.doi.org/10.3390/rs4051190.

Jakubowski M.K., Guo Q., Kelly M. (2013) - *Tradeoffs between lidar pulse density and forest measurement accuracy*. Remote Sensing of Environment, 130: 245-253. doi:

http://dx.doi.org/10.1016/j.rse.2012.11.024.

Kaartinen H., Hyyppä J., Yu X., Vastaranta M., Hyyppä H., Kukko A., Holopainen M., Heipke C., Hirschmugl M., Morsdorf F., Næsset E., Pitkänen J., Popescu S., Solberg S., Wolf B.M., Wu J.-C. (2012) - *An international comparison of individual tree detection and extraction using airborne laser scanning*. Remote Sensing, 4: 950-974. doi: http://dx.doi.org/10.3390/rs4040950.

Kitahara F., Mizoue N., Yoshida S. (2010) - *Effects of training for inexperienced surveyors on data quality of tree diameter and height measurements*. Silva Fennica, 44: 657-667. doi: http://dx.doi.org/10.14214/sf.133.

Lähivaara T., Seppänen A., Kaipio J.P., Vauhkonen J., Korhonen L., Tokola T., Maltamo M. (2014) - *Bayesian approach to tree detection based on airborne laser scanning data*. IEEE Transactions on Geoscience and Remote Sensing, 52: 2690-2699. doi: http://dx.doi.org/10.1109/TGRS.2013.2264548.

Lee H., Slatton K.C., Roth B.E., Cropper W.P. (2010) - *Adaptive clustering of airborne LiDAR data to segment individual tree crowns in managed pine forests*. International Journal of Remote Sensing, 31: 117-139. doi: http://dx.doi.org/10.1080/01431160902882561.

Lexerød N.L., Eid T. (2006) - *An evaluation of different diameter diversity indices based on criteria related to forest management planning*. Forest Ecology and Management, 222: 17-28. doi: http://dx.doi.org/10.1016/j.foreco.2005.10.046.

Li W., Guo Q., Jakubowski M.K., Kelly M. (2012) - *A new method for segmenting individual trees from the lidar point cloud*. Photogrammetric Engineering & Remote Sensing, 78: 75-84. doi: http://dx.doi.org/10.14358/PERS.78.1.75.

Lindberg E., Eysn L., Hollaus M., Holmgren J., Pfeifer N. (2014) - *Delineation of tree crowns and tree species classification from full-waveform airborne laser scanning data using 3-D ellipsoidal clustering*. IEEE Journal of Selected Topics in Applied Earth Observations and Remote Sensing, 7: 3174-3181. doi: http://dx.doi.org/10.1109/JSTARS.2014.2331276.

Lu X., Guo Q., Li W., Flanagan J. (2014) - *A bottom-up approach to segment individual deciduous trees using leaf-off lidar point cloud data*. ISPRS Journal of Photogrammetry and Remote Sensing, 94: 1-12. doi: http://dx.doi.org/10.1016/j.isprsjprs.2014.03.014.

Magnussen S., Næsset E., Gobakken T. (2010) - *Reliability of LiDAR derived predictors of forest inventory attributes: A case study with Norway spruce*. Remote Sensing of Environment, 114: 700-712. doi: http://dx.doi.org/10.1016/j.rse.2009.11.007.

McElhinny C., Gibbons P., Brack C., Bauhus J. (2005) - *Forest and woodland stand structural complexity: Its definition and measurement*. Forest Ecology and Management, 218: 1-24. doi: http://dx.doi.org/10.1016/j.foreco.2005.08.034.

Monnet J.M., Mermin È. (2014) - *Cross-correlation of diameter measures for the co-registration of forest inventory plots with airborne laser scanning data*. Forests, 5: 2307-2326. doi: http://dx.doi.org/10.3390/f5092307.

Morsdorf F., Meier E., Kötz B., Itten K.I., Dobbertin M., Allgöwer B. (2004) - *LIDAR-based geometric reconstruction of boreal type forest stands at single tree level for forest and wildland fire management*. Remote Sensing of Environment, 92: 353-362. doi: http://dx.doi.org/10.1016/j.rse.2004.05.013.

Næsset E. (2002) - *Predicting forest stand characteristics with airborne scanning laser using a practical two-stage procedure and field data*. Remote Sensing of Environment,

80: 88-99. doi: http://dx.doi.org/10.1016/S0034-4257(01)00290-5.

Neumann M., Starlinger F. (2001) - *The significance of different indices for stand structure and diversity in forests*. Forest Ecology and Management, 145: 91-106. doi: http://dx.doi.org/10.1016/S0378-1127(00)00577-6.

O'Hara K.L., Hasenauer H., Kindermann G. (2007) - *Sustainability in multi-aged stands: An analysis of long-term plenter systems*. Forestry, 80: 163-181. doi: http://dx.doi.org/10.1093/forestry/cpl051.

Ørka H.O., Dalponte M., Gobakken T., Næsset E., Ene L.T. (2013) - *Characterizing forest species composition using multiple remote sensing data sources and inventory approaches*. Scandinavian Journal of Forest Research, 28: 677-688. doi: http://dx.doi.org/10.1080/02827581.2013.793386.

Otsu N. (1979) - *A threshold selection method from gray-level histograms*. IEEE Transaction on Systems, Man and Cybernetics, 9: 62-66. doi: http://dx.doi.org/10.1109/TSMC.1979.4310076.

Packalen P., Strunk J.L., Pitkänen J.A., Temesgen H., Maltamo M. (2015) - *Edge-tree correction for predicting forest inventory attributes using area-based approach with airborne laser scanning*. IEEE Journal of Selected Topics in Applied Earth Observations and Remote Sensing, 8: 1274-1280. doi: http://dx.doi.org/10.1109/JSTARS.2015.2402693.

Pedersen R.Ø., Bollandsås O.M., Gobakken T., Næsset E. (2012) - *Deriving individual tree competition indices from airborne laser scanning*. Forest Ecology and Management, 280: 150-165. doi: http://dx.doi.org/10.1016/j.foreco.2012.05.043.

Persson Å., Holmgren J., Soderman U. (2002) - *Detecting and measuring individual trees using an airborne laser scanner*. Photogrametric Engineering & Remote Sensing, 68: 925-932.

Popescu S.C., Wynne R.H., Nelson R.F. (2002) - *Estimating plot-level tree heights with lidar: local filtering with a canopy-height based variable window size*. Computers and Electronics in Agriculture, 37: 71-95. doi: http://dx.doi.org/10.1016/S0168-1699(02)00121-7.

Pouliot D.A., King D.J., Pitt D.G. (2005) - *Development and evaluation of an automated tree detection - delineation algorithm for monitoring regenerating coniferous forests*. Canadian Journal of Forest Research, 35: 2332-2345. doi: http://dx.doi.org/10.1139/X05-145.

Reitberger J., Schnörr C., Krzystek P., Stilla U. (2009) - *3D segmentation of single trees exploiting full waveform LIDAR data*. ISPRS Journal of Photogrammetry and Remote Sensing, 64: 561-574. doi: http://dx.doi.org/10.1016/j.isprsjprs.2009.04.002.

Scrinzi G., Galvagni D., Marzullo L. (2010) - *I nuovi modelli dendrometrici per la stima delle masse assestamentali in Provincia di Trento*. Provincia Autonoma di Trento - Servizio Foreste e Fauna, Trento.

Shi J., Malik J. (2000) - *Normalized cuts and image segmentation*. IEEE Transactions on Pattern Analysis and Machine Intelligence, 22: 888-905. doi: http://dx.doi.org/10.1109/34.868688.

Solberg S., Næsset E., Bollandsås O.M. (2006) - *Single tree segmentation using airborne laser scanner data in a structurally heterogeneous spruce forest*. Photogrammetric Engineering & Remote Sensing, 72: 1369-1378. doi: http://dx.doi.org/0099-

1112/06/7212-1369.

Takahashi T., Yamamoto K., Senda Y., Tsuzuku M. (2005) - *Estimating individual tree heights of sugi (Cryptomeria japonica D. Don) plantations in mountainous areas using small-footprint airborne LiDAR.* Journal of Forest Research, 10: 135-142. doi: http://dx.doi.org/10.1007/s10310-004-0125-8.

Tang F.F., Zhang X.H., Liu J.N. (2007) - *Segmentation of tree crown model with complex structure from airborne LiDAR data.* Geoinformatics 2007: Remotely Sensed Data and Information, 67520A. doi: http://dx.doi.org/10.1117/12.760476.

Tang S., Dong P., Buckles B.P. (2013) - *Three-dimensional surface reconstruction of tree canopy from lidar point clouds using a region-based level set method.* International Journal of Remote Sensing, 34: 1373-1385. doi: http://dx.doi.org/10.1080/01431161.2012.720046.

Vasilescu M.M. (2013) - *Standard error of tree height using vertex III.* Bulletin of the Transilvania University of Braşov, Series II: Forestry, Wood Industry, Agricultural Food Engineering 6, 6.

Vauhkonen J., Ene L., Gupta S., Heinzel J., Holmgren J., Pitkanen J., Solberg S., Wang, Y., Weinacker H., Hauglin K.M., Lien V., Packalen P., Gobakken T., Koch B., Næsset E., Tokola T., Maltamo M. (2011) - *Comparative testing of single-tree detection algorithms under different types of forest.* Forestry, 85: 27-40. doi: http://dx.doi.org/10.1093/forestry/cpr051.

Wang Y., Weinacker H., Koch B. (2008) - *A lidar point cloud based procedure for vertical canopy structure analysis and 3D single tree modelling in forest.* Sensors, 8: 3938-3951. doi: http://dx.doi.org/10.3390/s8063938.

Woodcock C.E., Strahler A.H., Jupp D.L.B. (1988) - *The use of variograms in remote sensing: II. Real digital images.* Remote Sensing of Environment, 25: 349-379. doi: http://dx.doi.org/10.1016/0034-4257(88)90109-5.

Yao W., Krull J., Krzystek P., Heurich M. (2014) - *Sensitivity analysis of 3D individual tree detection from LiDAR point clouds of temperate forests.* Forests, 5: 1122-1142. doi: http://dx.doi.org/10.3390/f5061122.